Low-temperature structural transition in the quasi-one-dimensional spin- 1 2 compound L i2 C u2 O(SO 4)2

Gwenaelle Rousse, J. Rodríguez-Carvajal, C. Giacobbe, M. Sun, O. Vaccarelli, G. Radtke

Low-temperature structural transition in the quasi-one-dimensional spin-$\frac{1}{2}$ compound $Li_2Cu_2O(SO_4)_2$

G. Rousse,[1,2,3,*] J. Rodríguez-Carvajal,[4] C. Giacobbe,[5] M. Sun,[1,2] O. Vaccarelli,[6] and G. Radtke[6]

[1]*Collège de France, Chimie du Solide et de l'Energie, UMR 8260, 11 place Marcelin Berthelot, 75231 Paris Cedex 05, France*

[2]*Réseau sur le Stockage Electrochimique de l'Energie (RS2E), FR CNRS 3459, France*

[3]*Sorbonne Universités - UPMC Univ Paris 06, 4 Place Jussieu, F-75005 Paris, France*

[4]*Institut Laue-Langevin (ILL), CS 20156, 71 Avenue des Martyrs, 38042 Grenoble cedex 9, France*

[5]*ESRF, 71 Avenue des Martyrs, 38000 Grenoble, France*

[6]*Institut de Minéralogie, de Physique des Matériaux, et de Cosmochimie (IMPMC), Sorbonne Universités - UPMC Univ Paris 06, UMR CNRS 7590, Muséum National d'Histoire Naturelle, IRD UMR 206, 4 place Jussieu, F-75005 Paris, France*

(Received 15 January 2017; revised manuscript received 23 February 2017; published 5 April 2017)

A thorough structural exploration has been made on the quasi-one-dimensional $S = 1/2$ compound $Li_2Cu_2O(SO_4)_2$ by neutron and synchrotron x-ray diffraction. It reveals the occurrence of a structural transition at 125 K, characterized by a lowering of symmetry from $P4_2/m$ to $P\bar{1}$, which is possibly driven by an exchange striction mechanism. This transition involves a dimerization of some Cu in the edge-sharing tetrahedral Cu chains. A symmetry mode analysis indicates that one representation, $\Gamma_3{}^+\Gamma_4{}^+$, dominates the structural transition. Interestingly, no intermediate structure with $P112/m$ symmetry is observed experimentally. Lastly, temperature dependent magnetic susceptibility measurements and neutron diffraction reveal that the magnetic ground state of this compound is a spin-singlet with a spin gap, characterized by the absence of long-range magnetic order down to 1.7 K.

DOI: 10.1103/PhysRevB.95.144103

I. INTRODUCTION

Electronic and magnetic systems in which a dominant one-dimensional (1D) property exists have attracted a lot of interest in the last 40 years [1]. Spin-lattice interactions are often accompanied by exchange striction phenomena, such as spin-Peierls transitions and spin-driven Jahn-Teller effects. The Peierls transition appears in 1D conducting systems as an instability produced by interactions with phonons. At low temperature, the system becomes distorted producing a gap in the electronic bands and thus a metal-semiconductor or metal-insulator transition [2]. Analogously, spin-Peierls transitions are observed in certain quasi-one-dimensional antiferromagnets where spin phonon coupling results in a dimerization, forming spin singlets on dimers. In the magnetic excitation spectrum, the opening of a gap is concomitant with the structural transition and the ground state becomes non-magnetic. Well-known examples in spin-1/2 inorganic systems are TiOCl [3] or $CuGeO_3$ that has become the prototype of the spin-Peierls system [4,5]. The spin-driven Jahn-Teller mechanism has also recently attracted a lot of interest in the context of geometrically frustrated lattices, as a mechanism lifting the large degeneracy of their magnetic ground-state manifold. A seminal example is the pyrochlore structure, built on a three-dimensional arrangement of tetrahedra sharing vertexes as encountered in spinel-type compounds. The spin-driven Jahn-Teller mechanism is believed to be at the origin of the cubic to tetragonal transition in the spin-1 ZnV_2O_4 and MgV_2O_4 compounds [6]. In this paper, we describe a complex structural phase transition occurring in the quasi-1D spin-1/2 compound $Li_2Cu_2O(SO_4)_2$ displaying characteristics reminiscent of exchange striction mechanisms.

$Li_2Cu_2O(SO_4)_2$ has been synthetized for the first time in 2015 in the quest for new positive electrode materials for Li-ion batteries [7]. Beyond its electrochemical properties (it shows a high voltage activity at 4.7 V vs Li), this cuprate displays a very peculiar crystal structure that makes it a potential candidate for original low-dimensional magnetism. Indeed, Cu^{2+} ions form regular tetrahedral chains so that this compound can serve as a model for studying quasi-1D magnetism. In this paper, we report for the first time the magnetic behavior of $Li_2Cu_2O(SO_4)_2$, and we show that the susceptibility displays a behavior typical of a 1D antiferromagnet with a spin singlet ground state. We reveal the existence of a structural phase transition at 125(5) K and solve the low-temperature structure using x-ray synchrotron and neutron powder diffraction. The structural relationships between the room-temperature tetragonal phase and the low-temperature triclinic phase are analyzed in terms of symmetry-adapted modes. Moreover, neutron magnetic scattering was employed to confirm the absence of long-range magnetic ordering down to 1.7 K.

II. EXPERIMENTAL DETAILS

A. Synthesis

$Li_2Cu_2O(SO_4)_2$ was obtained from Li_2O (Alfa Aesar, 99.5%) and $CuSO_4$ (Alfa Aesar, Reagent grade) according to the reaction $Li_2O + 2\,CuSO_4 \rightarrow Li_2Cu_2O(SO_4)_2$. The dried Li_2O and $CuSO_4$ powders were ball milled for one hour into an Ar-filled ball-mill jar with a stainless-steel ball/powder weight ratio of 20. The resulting mixture was placed in an alumina boat and annealed at 400 °C for 4 days under Ar. $Li_2Cu_2O(SO_4)_2$ is obtained as an emerald-green powder.

*Corresponding author: gwenaelle.rousse@upmc.fr

B. X-Ray and neutron diffraction

The structure of $Li_2Cu_2O(SO_4)_2$ was explored by complementary synchrotron x-ray diffraction data (XRD) recorded in transmission mode ($\lambda = 0.354688$ Å, capillary 0.7 mm diameter) at the ID22 beamline at ESRF (Grenoble, France) and neutron powder diffraction data ($\lambda = 1.541946$ Å, high-resolution mode, take-off angle 90°) measured at the D20 neutron diffractometer at Institut Laue Langevin (Grenoble, France). A neutron wavelength of 2.42 Å was also used to explore a possible magnetic ordering. For neutron experiments, the powder was placed in a 7-mm-diameter cylindrical vanadium can. All powder patterns were refined using the Rietveld method [8] as implemented in the FULLPROF program [9,10]. AMPLIMODES [11], available from the Bilbao Crystallographic Server, was used for generating the input control file for FULLPROF to perform refinements using symmetry-mode analysis.

C. Magnetization and specific heat measurements

The temperature dependence of the magnetization was measured using a SQUID (XL, Quantum Design), under a magnetic field of 5000 Oe. Specific heat measurements were made on a cylindrical pellet (~20 mg of powder sintered for 48 h at 400 °C under Ar) using a Physical Properties Measurement System (PPMS) from Quantum Design.

D. Differential scanning calorimetry

Differential scanning calorimetry (DSC) experiments were performed using a SENSYS evo DSC apparatus from Setaram, on ~40 mg of powder. The measurement was performed under inert gas, with heating and cooling rates of 5 K/min.

III. RESULTS

A. Magnetic susceptibility of $Li_2Cu_2O(SO_4)_2$

The room-temperature structure of $Li_2Cu_2O(SO_4)_2$ was solved from combined neutron/synchrotron x-ray powder diffraction in 2015 [7]. The structure has a tetragonal symmetry, with space group $P4_2/m$, and structural details are reported in the next section. Spin-1/2 are held by Cu^{2+} ions forming chains oriented along the **c** axis of the crystal and well separated from each other by Li ions and SO_4 tetrahedral groups. These chains are built from a stacking of two edge-sharing CuO_4 squares forming $[Cu_2O_6]$ dimers denoted platelets thereafter. The latter are connected one to each other through an oxygen atom, after being rotated by 90° under the effect of the 4_2 helical axis; this leads to infinite "Cu_2O_5" chains running along [001] [Fig. 1(a)]. If one considers copper atoms only and draws the Cu-Cu bonds, the resulting topology consists of edge-sharing tetrahedral chains [Fig. 1(b)]. The atomic structure of this compound exhibits therefore possible magnetic frustration and strong 1D characteristics.

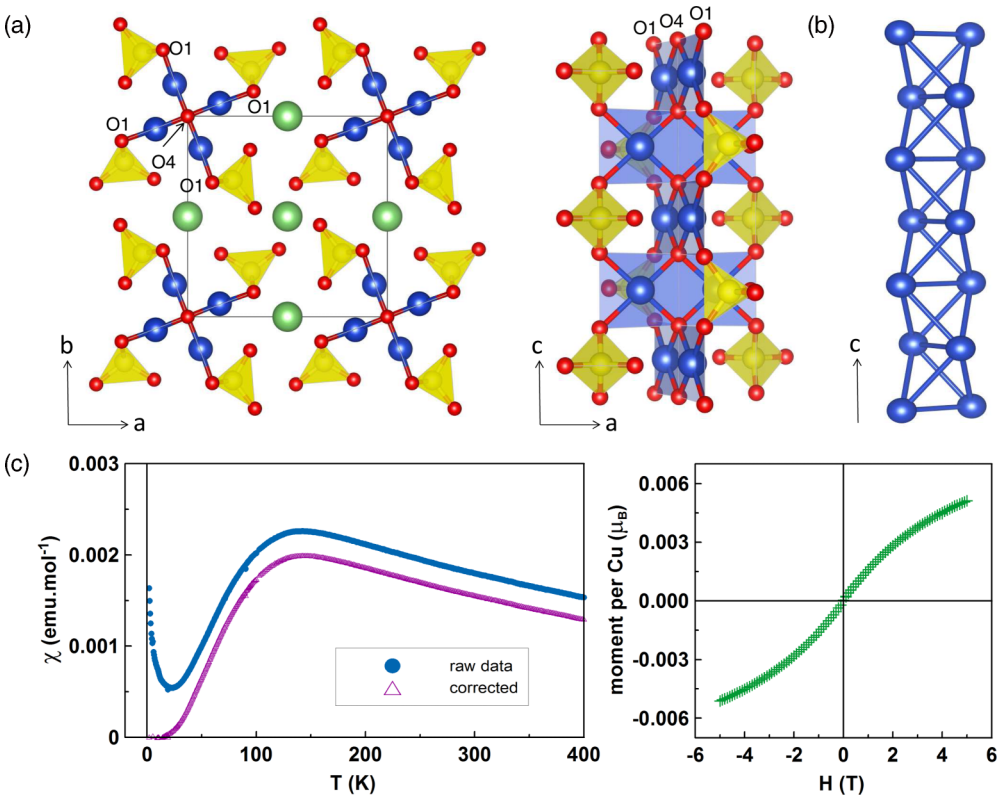

FIG. 1. (a) Structure of $Li_2Cu_2O(SO_4)_2$. Li is green, Cu is blue, O is red, SO_4 tetrahedral groups are colored in yellow. Oxygen atoms coordinating Cu in CuO_4 are labelled (O1 and O4). The right panel shows a "Cu_2O_5" chain running along [001] (b) Cu framework. Only Cu-Cu bonds are shown, forming edge-sharing Cu tetrahedral 1D chains along [001]. (c) Susceptibility (under 5000 Oe, field cooled and zero field cooled superimpose) and magnetization curve at $T = 3$ K. The raw susceptibility (blue circles) was corrected from a paramagnetic and temperature independent contributions (see text), to obtain the $Li_2Cu_2O(SO_4)_2$ susceptibility (purple triangles).

Magnetic susceptibility measurements were conducted between 2 and 400 K, under 5000 Oe, and a magnetization curve was recorded at 3 K under fields up to 50 kOe [Fig. 1(c)]. The susceptibility shows a smooth increase down to 150 K, followed by a smooth decrease and a subsequent sharp increase at very low temperature. The latter varies in amplitude from one batch to another and likely arises from a small amount of paramagnetic impurities. We have shown in our previous study [7] that Li_2SO_4 and $CuSO_4$ are likely impurities. Therefore the experimental susceptibility has been corrected from both the paramagnetic tail, fitted through a Curie Weiss law, $\chi_{imp} = \frac{C_{imp}}{T-\theta_{imp}}$, where C_{imp} and θ_{imp} are, respectively, the Curie-Weiss constant and temperature of the impurity, and from a temperature-independent contribution χ_0 arising from the sample holder and core diamagnetism of the compound. The following values were used: $\chi_0 = 2.2.10^{-4}$ emu mol^{-1}, $\theta_{imp} = -2.6$ K, and $C_{imp} = 6.4 \times 10^{-3}$ emu K mol^{-1}. These contributions were then subtracted from the total susceptibility, to obtain a signal coming from $Li_2Cu_2O(SO_4)_2$ only. The resulting susceptibility, with a broad maximum around 130–140 K, is typical for a 1D antiferromagnetic system, with a spin-singlet ground-state and a spin-gapped behavior. This is further confirmed by the magnetization curve which shows a typical antiferromagnetic behavior, without any hysteresis.

However, before engaging in a thorough study of the magnetic properties, it is of utmost importance to check the structural behavior of $Li_2Cu_2O(SO_4)_2$ below room temperature, in order to spot possible structural transitions. Indeed, many Cu^{2+}-based compounds present structural distortions at low temperature, such as the spin-Peierls transition in $CuGeO_3$ [1,2]. The aim of the next section is to investigate, via complementary synchrotron x-ray and neutron powder diffraction, the structural features of $Li_2Cu_2O(SO_4)_2$ down to 2 K.

B. Tetragonal to triclinic phase transition on cooling

At room temperature, $Li_2Cu_2O(SO_4)_2$ crystallizes in the previously reported tetragonal structure, as demonstrated by the combined refinement of synchrotron x-ray (ID22 diffractometer) and neutron powder diffraction patterns (D20 diffractometer) in Figs. 2(a) and 2(b). The refinement was conducted in the $P4_2/m$ space group, with all atoms distributed among eight crystallographic sites. Absorption corrections $\mu R = 0.38$ and 0.19 were applied for neutrons and x-ray refinements, respectively. All atomic positions and isotropic temperature factors were refined without any constraints. The background was modeled with Chebyshev polynomials. For the synchrotron pattern, anisotropic strain parameters were refined taking into account the tetragonal symmetry. The following values of S_{hkl}, using the Stephens notation [12], were obtained: $S_{400} = 0.086(3), S_{004} = 0.46(3), S_{220} = 0.196(8)$, and $S_{202} = 2.37(3)$ [13]. The corresponding strain is anisotropic and varies between $\sim 9.10^{-4}$ and $\sim 22.10^{-4}$ depending on the direction in reciprocal space (see document 1 (microstructural file) in Ref. [14]). These values indicate the presence of fluctuations and correlations in the tetragonal lattice parameters [15]. On another side, no size broadening effects were detected from the refinement. Table I gathers the structural parameters obtained from the refinement. Li atoms sit in $2d$ and $2f$ Wyckoff positions. The former position, occupied with Li1, is octahedrally coordinated with O1 and O2 oxygen atoms, while the latter, occupied with Li2, is in the middle of a tetrahedron made of O3 oxygen atoms. All O1, O2, and O3 are also part of a SO_4 tetrahedron. O4 is the only oxygen atom not being linked to a sulfur atom. It is on the $2e$ Wyckoff position and bridges the four copper atoms of the unit cell which are placed on the $4j$ position. Cu^{2+} is therefore surrounded by two O1 and two O4 oxygen atoms, so as to form a square planar coordination commonly observed for this Jahn-Teller ion. The room-temperature tetragonal structure of $Li_2Cu_2O(SO_4)_2$ is shown in Fig. 1(a).

Structural evolution down to 2 K was first monitored using synchrotron x-ray diffraction so as to spot tiny structural distortions. Indeed, neutron diffraction at continuous sources displays Bragg peaks whose intrinsic broadening is much larger. Two batches of $Li_2Cu_2O(SO_4)_2$ were therefore measured at the Synchrotron powder diffraction beamline ID22 at ESRF. The first one was performed in an explorative way, from 300 to 4 K, and the second was measured every 5 K from 100 to 125 K. Selected regions of the collected patterns versus temperature are shown in Fig. 3. $Li_2Cu_2O(SO_4)_2$ keeps the tetragonal structure down to 130 K, with, however, a progressive increase of anisotropic strain broadening on cooling. At 125 K, some (hkl) reflections split and the splitting expands continuously on cooling down to 4 K. The relative intensities remain similar between the high and the low-temperature phase, so that this behavior is typical of a displacive transition, which can be described with group-subgroup relationships, as will be shown later. As the unit cell distortion increases when the temperature is decreased, we chose the pattern recorded at 4 K to solve the low-temperature structure. Our initial attempts to solve the low-temperature phase in subgroups of high symmetry from $P4_2/m$ (e.g., of monoclinic symmetry) all failed, and we figured out that only a triclinic cell can account for the complex splitting of the reflections. This triclinic cell has the same metrics in unit cell parameters, and same origin, as the tetragonal cell. The structure was then refined in the $P\bar{1}$ space group, starting from atomic positions from the high-temperature $P4_2/m$ phase. Figure 4 shows the way atoms of the high-temperature tetragonal structure are transformed into the $P\bar{1}$ triclinic cell. Atoms are distributed among 16 crystallographic sites: 3 sites for Li, 2 for Cu, 2 for S, and 9 for O. All of them are in general position $2i$ except Li1 and Li2, which are in $1d$ and $1g$, respectively. Figures 2(c) and 2(d) show the result of a combined synchrotron/neutron diffraction refinement, the former being measured at 4 K (the minimum temperature the cryostat on ID22 could reach), the latter at 2 K. This way, the structure can be assessed with confidence as the extreme resolution of the synchrotron allows a precise determination of the lattice parameters, while neutron diffraction provides accurate atomic positions, with a particularly favorable contrast for light atoms Li (–1.90 fm), S (+2.847 fm), and O (+5.803 fm) compared to the heavy Cu (+7.718 fm). The isotropic temperature factors were imposed equal for each chemical species and lattice parameters were allowed to vary independently to account for the difference in temperature. The refined atomic positions and structure parameters for the low-temperature triclinic phase are gathered in Table II.

The low-temperature structure is plotted in Fig. 5(a) superimposed with the structure at 300 K shown with gray atoms.

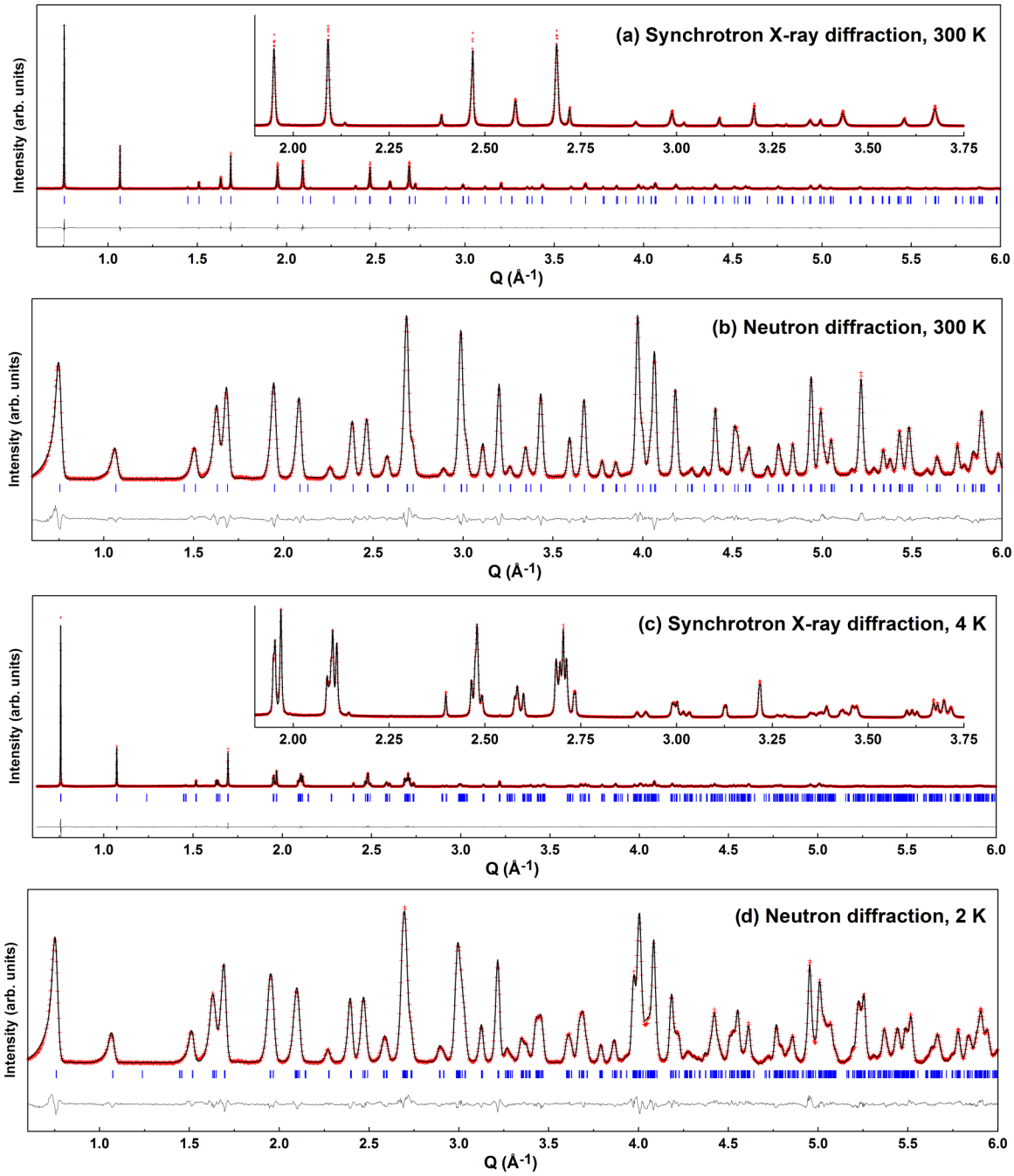

FIG. 2. Rietveld refinement of synchrotron (a, c), and neutron (b, d) diffraction patterns of $Li_2Cu_2O(SO_4)_2$ at $T = 300$ K and at $T = 4$ K (synchrotron)/2 K (neutrons). The red crosses, black continuous line, and bottom green line represent the observed, calculated, and difference patterns, respectively. Vertical blue tick bars mark the reflection positions. All patterns are plotted vs Q to allow for a direct comparison between patterns recorded with different wavelengths.

It appears clearly that both structures are very close to each other. In particular, Li positions are almost superimposable, so are O2, O3 and O4 atoms (labels refer to the tetragonal description). O1, S, and to a lesser extent Cu appear to experience the largest displacements, so that the symmetry breaking induces a tilt in the Cu_2O_6 platelets, as highlighted by arrows in Fig. 5(b). Cu_2O_6 platelets in the Cu_2O_5 chains are therefore no longer perpendicular to [001]. Even though atomic displacements are small, this transition has important effects on the Cu-Cu framework. The edge-sharing Cu_4 tetrahedra become distorted, as can be observed in Fig. 5(c). At 300 K, interplatelet bonds have all the same length imposed by symmetry [3.2602(7) Å], whereas the intraplatelet bond, perpendicular to [001], and shared between two adjacent tetrahedra, is 2.8816(10) Å. The triclinic distortion leads to six individual distances for each tetrahedron. The edge-sharing Cu-Cu intraplatelet distance is split into two, with distances of 2.8744(19) Å (Cu1-Cu1) and 2.8833(18) Å (Cu2-Cu2), echoing the splitting of Cu into Cu1 and Cu2. The splitting in distances is more severe for the four previously equivalent

TABLE I. Structural parameters for $Li_2Cu_2O(SO_4)_2$, deduced from the combined Rietveld refinement of the Synchrotron XRD and neutron diffraction patterns at 300 K. A bond valence sum analysis (BVS) is also reported for each atom. The crystallographic information file (CIF) is available in [14].

$Li_2Cu_2O(SO_4)_2$, high-temperature phase
Space Group: $P4_2/m$
$a = 8.324560(12)$ Å, $c = 5.089952(14)$ Å, $V = 352.725(1)$ Å^3

Atom	Wyckoff site	x	y	z	B (Å^2)	BVS
Li1	2*d*	0	0.5	0.5	2.6(2)	0.91(2)
Li2	2*f*	0.5	0.5	0.25	0.56(14)	1.23(3)
Cu	4*j*	0.16055(9)	0.06465(8)	0	0.554(11)	2.05(3)
S	4*j*	0.31687(17)	0.22596(16)	0.5	0.60(2)	6.08(2)
O1	8*k*	0.32953(19)	0.12343(16)	0.7375(3)	1.28(3)	2.02(2)
O2	4*j*	0.1687(3)	0.3128(2)	0.5	0.96(4)	2.05(2)
O3	4*j*	0.4570(2)	0.3359(3)	0.5	0.59(4)	2.08(2)
O4	2*e*	0	0	0.25	0.40(6)	2.03(2)

Reliability parameters: $\chi^2 = 4.17$;
Neutrons: Bragg R-factor = 3.33%, Rf-factor = 2.08%;
Synchrotron: Bragg R-factor = 4.51%, Rf-factor = 5.56%

interplatelet bonds: the shortest, shown in yellow in Fig. 5(c), has a distance of 3.139(3) Å, and the longest (shown in red) has a distance of 3.363(3) Å. The phase transition is therefore accompanied by a dimerization of Cu.

Lastly, for sake of completion, all synchrotron x-ray diffraction patterns were refined using this triclinic cell up to 125 K, and with the tetragonal cell between 130 and 300 K. The lattice parameter evolution is shown in Fig. 6 and shows that the triclinic distortion gets larger on cooling, as already guessed from examination of the peaks splitting (Fig. 3). It also highlights the reproducibility of the phenomenon as the second diffraction experiment, performed in the range 100 to 130 K, nicely matches the first one (lattice parameters marked with crosses).

Finally, Fig. 6 also reports the evolution of the unit cell volume versus temperature. It is worth noting that, within the experimental error, the tetragonal-triclinic transition is not accompanied by a discontinuous change in the unit cell volume.

C. Symmetry mode analysis and symmetry around the transition

The conventional Rietveld refinements shown above seem to indicate the absence of a domain in temperature for which the structure would be an intermediate between tetragonal and triclinic. This comes as a surprise since phase transitions usually occur according to direct group → maximal subgroup

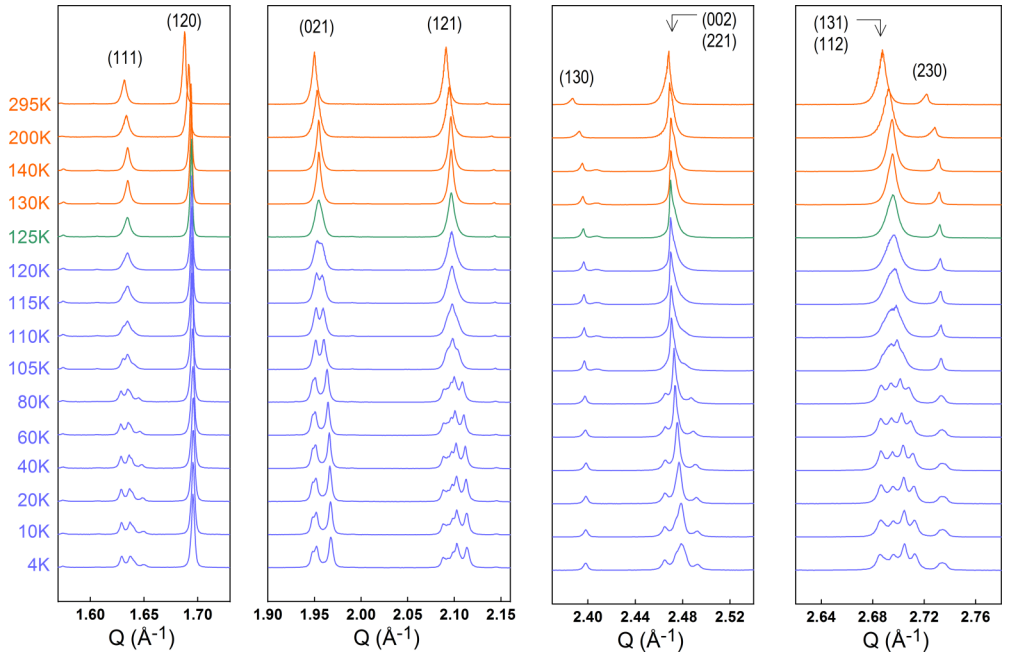

FIG. 3. Evolution of the synchrotron x-ray powder patterns of $Li_2Cu_2O(SO_4)_2$ between 295 and 4 K. Note the splitting of some (*hkl*) reflections when the temperature is decreased below 125 K (green pattern).

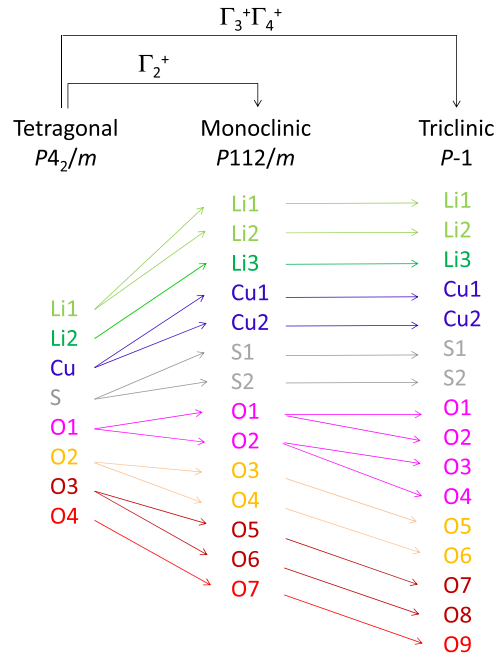

FIG. 4. Deduction of atomic positions from the tetragonal to the triclinic structure, and via the possible intermediate monoclinic phase (not experimentally observed, see text) and the representations associated with those transitions.

transitions. In the present case, the triclinic phase ($P\bar{1}$) is actually a subgroup of $P112/m$, which is in turn a subgroup of $P4_2/m$. In this section, we reexamine refinements using symmetry mode analysis, and we explore the possibility of having an intermediate $P112/m$ structure in between the tetragonal and triclinic structures.

A symmetry mode analysis was conducted on the triclinic low-temperature phase using the AMPLIMODES program available on the Bilbao Crystallographic Server. This analysis consists in decomposing the symmetry-breaking distortion present in the distorted structure (triclinic) into contributions from different symmetry-adapted modes. This approach has been shown to be very useful for establishing the driving mechanisms of structural phase transitions or the fundamental instabilities at the origin of the distorted phases [11]. AMPLIMODES produces input files for FULLPROF and, using this last program, the amplitudes of the symmetry modes can be refined [11,16].

To materialize this, we use the high-temperature tetragonal atomic positions at 300 K and describe the structure at 2 K by (i) applying the $P\bar{1}$ distortion to the lattice parameters and (ii) refining the amplitudes of the modes determined by AMPLIMODES. We used this strategy as a combined refinement on the 2 K/neutron and 4 K/synchrotron patterns.

Three effective representations, Γ_1^+, Γ_2^+ and the combination $\Gamma_3^+\Gamma_4^+$ have to be considered for the symmetry transition from $P4_2/m$ to $P\bar{1}$. The latter two one-dimensional representations are grouped together as they are degenerate, this extra degeneracy being brought by time reversal symmetry. 11 modes transform according to Γ_1^+, 13 according to Γ_2^+, and 18 according to $\Gamma_3^+\Gamma_4^+$. Refining the amplitudes of all modes led to a refinement with a similar quality as the conventional Rietveld refinement. Modes for which the amplitude was refined to a value that includes zero within the standard deviation were arbitrary fixed to zero. The input pcr-file used for the refinement with FULLPROF with description of all 42 individual modes and their final refined amplitudes is reported in Ref. [14], Tables SI1 and SI2. It highlights that modes with Γ_1^+ and Γ_2^+ representations are obtained with relatively small amplitudes, while modes with the largest amplitudes have the $\Gamma_3^+\Gamma_4^+$ symmetry. The displacements corresponding to each symmetry mode are drawn with arrows proportional to the refined amplitudes in Fig. 7 (only those affecting Cu and O are shown for clarity) and the overall amplitude of each representation is also reported. The expressions used for calculating the displacement vectors and the global amplitudes corresponding to the effective representations are provided in Appendix. The Γ_1^+ representation involves a rotation of Cu_2O_6 platelets around [001] whereas the Γ_2^+ one involves a translation of the bridging oxygen atoms sitting on the fourfold axis (and not being part of a sulfate group) so as to obtain alternate compressed and expanded Cu_2O_6 groups along [001]. The largest amplitude is associated with the $\Gamma_3^+\Gamma_4^+$ representation and corresponds to a tilt of the Cu_2O_6 platelets deforming the Cu_4 tetrahedra, leading to the shortening of certain Cu-Cu bonds and the increase of others, as discussed above. Lastly, note that the amplitudes deduced from the refinement using symmetry mode analysis perfectly match the displacements which were deduced from the direct comparison of the two tetragonal and triclinic structures shown in Fig. 5.

The transition from $P4_2/m$ to $P\bar{1}$ is therefore not a transition from a group into a maximum subgroup: it involves an index 4. Looking at the group/subgroups relations, one would expect the following sequence, which involves two successive transitions of index 2:

$$P4_2/m \rightarrow P2/m \rightarrow P\bar{1}.$$

Therefore we aimed at examining the possibility of having an intermediate domain in temperature at which the structure could be of monoclinic symmetry. In order to keep the same lattice unit cell vectors, the monoclinic cell was here described in a non-standard description, i.e., $P112/m$. This allows for a direct comparison of the three tetragonal, monoclinic, and triclinic structural models. In particular, the patterns recorded at 120 and 130 K, just around the transition, were examined with special care, in order to check whether the monoclinic structure could be a better choice. To do so, we used the same approach of symmetry mode analysis as described above, in order to reduce the number of parameters to refine. The high-temperature tetragonal structure was therefore implemented with monoclinic lattice parameters, and amplitudes of symmetry-allowed modes were refined. The symmetry analysis leads to two representations, Γ_1^+ and Γ_2^+, each having 11 and 13 modes, respectively. Figures 8(a) and 8(b) show the refinement of the 120 K synchrotron XRD pattern using the triclinic $P\bar{1}$ and the monoclinic $P112/m$ models. Enlargements on some specific reflections clearly indicate that the triclinic symmetry is preferred, see, for example, how the splitting of the (021) reflection (zone 2) is better reproduced in triclinic than in the monoclinic symmetry. At 130 K, the splitting of some reflections has obviously disappeared and

TABLE II. Structural parameters for $Li_2Cu_2O(SO_4)_2$, deduced from the combined Rietveld refinement of the Synchrotron XRD at 4 K and neutron diffraction patterns at 2 K. A bond valence sum analysis (BVS) is also reported for each atom. The crystallographic information file (CIF) is available in [14].

$Li_2Cu_2O(SO_4)_2$, low-temperature phase
Space Group: $P\bar{1}$
Synchrotron, 4 K:
$a = 8.29197(3)$ Å, $b = 8.27975(2)$ Å, $c = 5.06688(2)$ Å,
$\alpha = 90.4362(3)$ deg., $\beta = 90.5984(3)$ deg., $\gamma = 90.0666(3)$ deg.
$V = 347.839(2)$ Å^3
Neutrons, 2 K:
$a = 8.2889(6)$ Å, $b = 8.2791(6)$ Å, $c = 5.07645(4)$ Å,
$\alpha = 90.4332(17)$ deg., $\beta = 90.5385(16)$ deg., $\gamma = 90.0838(13)$ deg.
$V = 348.34(4)$ Å^3

Atom	Wyckoff site	x	y	z	B (Å^2)	BVS
Li1	1*d*	1/2	0	0	0.42(12)	0.95(2)
Li2	1*g*	0	1/2	1/2	0.42(12)	0.96(2)
Li3	2*i*	0.5048(15)	0.5039(16)	0.753(3)	0.42(12)	1.22(2)
Cu1	2*i*	0.16085(16)	0.06400(17)	0.0209(3)	0.17(2)	2.12(2)
Cu2	2*i*	0.93570(17)	0.16156(15)	0.4899(3)	0.17(2)	2.02(2)
S1	2*i*	0.3196(3)	0.2250(3)	0.5278(6)	0.25(3)	5.91(2)
S2	2*i*	0.7764(4)	0.3207(3)	0.9921(6)	0.25(3)	6.02(2)
O1	2*i*	0.3362(5)	0.1372(6)	0.7831(9)	0.205(17)	2.04(2)
O2	2*i*	0.6751(5)	0.8955(6)	0.6918(9)	0.205(17)	1.95(2)
O3	2*i*	0.8950(5)	0.3300(5)	0.2161(9)	0.205(17)	1.98(2)
O4	2*i*	0.1389(6)	0.6660(5)	0.2623(9)	0.205(17)	2.05(2)
O5	2*i*	0.8322(5)	0.6877(5)	0.4832(8)	0.205(17)	1.96(2)
O6	2*i*	0.6867(5)	0.1712(5)	0.0089(8)	0.205(17)	1.97(2)
O7	2*i*	0.4614(6)	0.3331(5)	0.5043(8)	0.205(17)	2.06(3)
O8	2*i*	0.6674(5)	0.4604(6)	0.0118(9)	0.205(17)	2.18(3)
O9	2*i*	−0.0032(5)	0.9902(5)	0.2440(9)	0.205(17)	2.094(13)

Reliability parameters: $\chi^2 = 3.67$;
Neutrons: Bragg R factor = 2.20%, Rf factor = 1.18%;
Synchrotron: Bragg R factor = 3.71%, Rf factor = 2.90%

we tried to refine the data both in monoclinic and tetragonal symmetries [Figs. 8(c) and 8(d)]. In both cases, anisotropic strain had to be taken into account for obtaining a good refinement. The refinement using the monoclinic description leads to lattice parameters $a = 8.29666(3)$ Å, $b = 8.29294(2)$ Å, $c = 5.086349(14)$ Å, and $\beta = 89.9942(6)^\circ$, while for the tetragonal description, we obtain $a = 8.294430(19)$ Å and $c = 5.086360(15)$ Å. The structural model with a monoclinic description is reported in Table III. The metrics of the monoclinic cell is therefore extremely close to the tetragonal lattice parameters (less than 0.02%). Moreover, the improvement in the quality of the refinement in the monoclinic description, which is directly linked to a larger number of variable/refined parameters, is not so important when compared to the

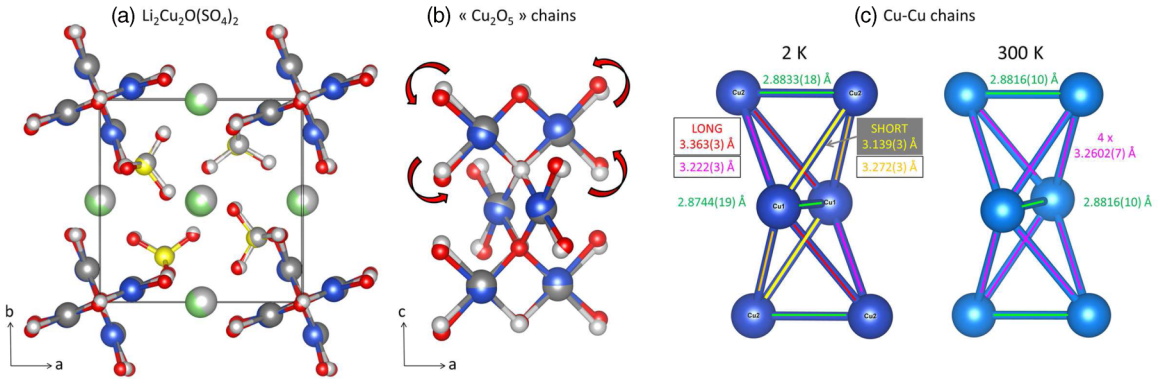

FIG. 5. (a) and (b) Superposition of the room temperature tetragonal and low-temperature triclinic structures of $Li_2Cu_2O(SO_4)_2$. The structure of the low-temperature triclinic phase at 2 K is shown with colors: Cu is blue, Li is green, S is yellow, and O is red. The atoms shown in gray are those of the room temperature tetragonal phase. (c) View of the edge-sharing Cu tetrahedral chains at 2 and 300 K, with Cu-Cu distances reported.

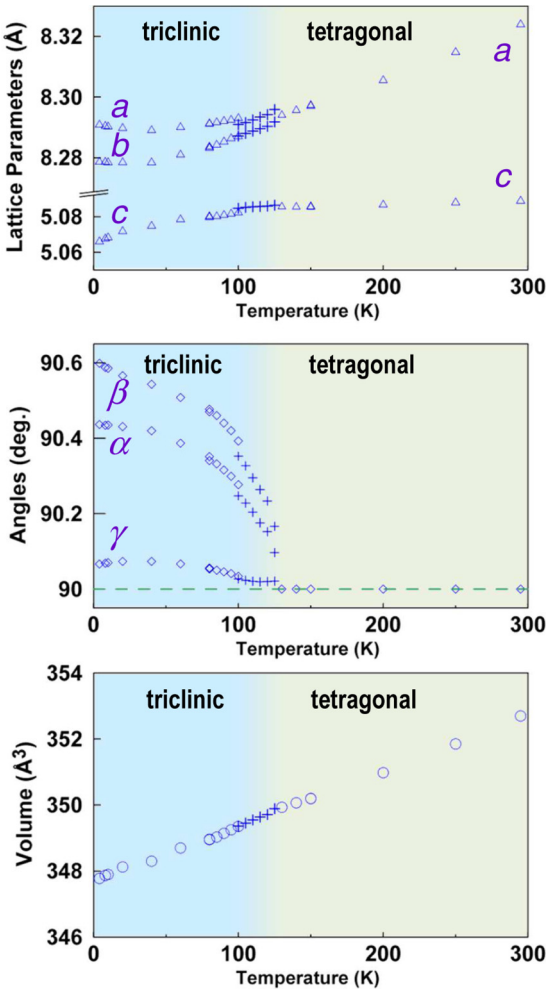

FIG. 6. Evolution of the lattice parameters and unit cell volume versus temperature, deduced from the synchrotron x-ray diffraction Rietveld refinements. Open symbols correspond to a first experiment while crosses are used for a second batch measured in the 100–130 K range.

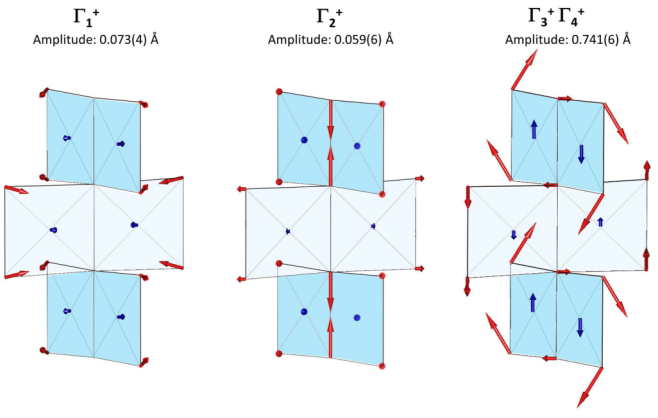

FIG. 7. Visualization of the atomic displacements of Γ_1^+, Γ_2^+ and $\Gamma_3^+\Gamma_4^+$ symmetries accounting for the $P4_2/m$ to $P\bar{1}$ structural transition. Only the effects on the Cu_2O_5 chains are displayed here (Cu is in the middle of the square planar entities built on oxygen atoms). Arrows correspond to the displacement vectors (blue for Cu atoms, red for oxygen atoms), with moduli proportional to the refined amplitude. The global amplitude is reported of each representation.

refinement performed using a tetragonal description. Therefore, at this stage, our data do not reveal any monoclinic domain, although it cannot be excluded neither.

At this point, we conjectured that measuring the heat capacity and the differential scanning calorimetry versus temperature could reveal (i) the order of the transition and (ii) whether one or two successive phase transitions are seen, i.e., shed light on the occurrence of the monoclinic structure. The specific heat C_p of $Li_2Cu_2O(SO_4)_2$ was measured between 2 and 300 K on heating, and from 170 to 90 K on cooling (without any magnetic field). C_p continuously increases versus T, indicating that the entropy associated to the transition is not detectable (Ref. [14], Fig. 1(a)); the absence of any lambda-shaped anomaly at the transition, which is expected for a second-order transition, suggests that the transition would be of first order. However, differential scanning calorimetry (Ref. [14], Fig. 1(b)), performed under Ar at a 5 K/min rate between room temperature and 110 K (the lowest possible temperature with the apparatus), does not exhibit any transition neither or, more precisely, the heat exchange associated with the transition is not detectable with our experimental setup. We therefore speculate that $Li_2Cu_2O(SO_4)_2$ might undergo a weak first order transition.

For sake of completion, we performed high intensity neutron powder diffraction at 2.42 Å, a wavelength suitable to study long range magnetic ordering. Patterns recorded between RT and 1.7 K showed, however, no appearance of additional peaks of magnetic origin (Fig. 9). Magnetic moments carried by Cu^{2+} ($S = 1/2$) are therefore not long-range ordered, in agreement with the susceptibility results and a singlet ground state. The background also did not increase at low temperature, so that no diffuse scattering is seen resulting from possible short range magnetic interactions.

D. Discussion and conclusion

In this paper, we have revealed the occurrence of a continuous structural phase transition at 125 K in $Li_2Cu_2O(SO_4)_2$, from a tetragonal to a triclinic structure. The latter was fully solved and described using symmetry mode analysis. It was shown that atomic displacements associated with the transition have a dominant component of $\Gamma_3^+\Gamma_4^+$ symmetry. The low-temperature triclinic structure shows a shortening of certain Cu-Cu bonds concomitant with an elongation of others. This displacive transition is not accompanied by any volume change, nor any measurable enthalpy, and shows no peak in specific heat measurements. Therefore it may be a weak first-order transition. Although surprising at first sight, it is not unusual that phase transitions are difficult to classify, and this point could be clarified once single crystals are available.

The second intriguing point is the apparent absence of a temperature domain into which the structure would adopt a monoclinic symmetry, between the tetragonal and triclinic ones. The symmetry mode analysis reveals that the dominant component of the atomic displacements involved in the transition from $P4_2/m$ to $P\bar{1}$ is of $\Gamma_3^+\Gamma_4^+$ symmetry whereas this representation is absent in a potential $P4_2/m$ to $P112/m$ transition, which involves Γ_2^+ only (Fig. 4). The driving force leading to this transition is not straightforward to identify. A number of possibilities can be safely excluded

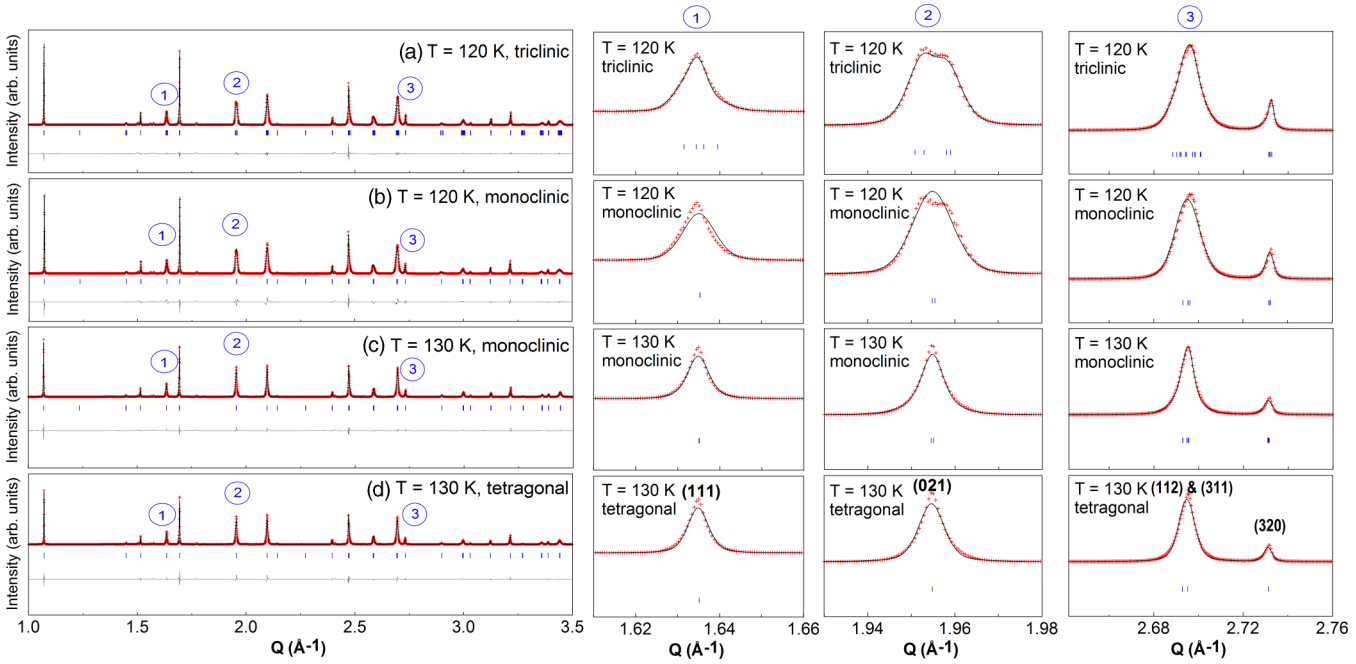

FIG. 8. Rietveld refinements of synchrotron x-ray powder diffraction patterns of $Li_2Cu_2O(SO_4)_2$ at $T = 120$ K [(a) and (b)] and $T = 130$ K [(c) and (d)]. At $T = 120$ K, two models are considered: triclinic $P\bar{1}$ (a) and monoclinic $P112/m$ (b), and at $T = 130$ K monoclinic $P112/m$ (c) and tetragonal $P4_2/m$ (d). The three panels on the right (numbered 1, 2, and 3) show enlargements of some reflections as indicated with the same numbering in the first column. The red crosses, black continuous line and bottom green line represent the observed, calculated, and difference patterns, respectively. Vertical blue tick bars mark the reflection positions.

however, and in particular those involving electronic degrees of freedom. A collective Jahn-Teller effect, occurring in other low dimensional spin-1/2 systems such as $Sr_3Cr_2O_8$ [17,18], can be trivially excluded as Cu^{2+} already occupies an atomic site with a square planar geometry, lifting the orbital degeneracy responsible for such phenomena. Charge ordering, met in mixed valence compounds such as α'-NaV_2O_5 [19–21], is also very unlikely to occur in this compound where the local environment and the formal valence of the Cu ions are well defined. This is confirmed by bond valence sum calculations, which do not show any significant charge imbalance below the structural transition (Tables I and II).

A mechanism related to symmetric exchange striction might therefore be at the origin of the observed distortion. This hypothesis is supported by the peculiar arrangement of the magnetic ions in the chains, which might give rise to geometric frustration. One should also strengthen the weakness of the atomic displacements involved in this transition and the resulting Cu-Cu dimerization occurring along the chains, which bears some similarities with systems showing a spin

TABLE III. Structural model of $Li_2Cu_2O(SO_4)_2$ in a monoclinic description as an hypothetical structure at 130 K.

Space Group: $P112/m$
$a = 8.29666(3)$ Å, $b = 8.29294(2)$ Å, $c = 5.086349(14)$ Å, $b = 89.9942(6)^\circ$
$V = 347.839(2)$ Å^3

Atom	Wyckoff site	x	y	z	B (Å^2)
Li1	1*c*	1/2	0	0	1.0(2)
Li2	1*e*	0	1/2	1/2	1.0(2)
Li3	2*l*	1/2	1/2	0.779(5)	1.0(2)
Cu1	2*m*	0.1592(3)	0.0648(3)	0	0.40(5)
Cu2	2*n*	0.9374(3)	0.1642(3)	1/2	0.40(5)
S1	2*n*	0.3161(7)	0.22518(19)	1/2	0.61(6)
S2	2*m*	0.77482(19)	0.3242(7)	0	0.61(6)
O1	4*o*	0.3284(9)	0.1189(9)	0.7272(13)	0.56(5)
O2	4*o*	0.8770(9)	0.3365(9)	0.2436(13)	0.56(5)
O3	2*n*	0.1716(4)	0.3169(12)	1/2	0.56(5)
O4	2*m*	0.6913(12)	0.1716(4)	0	0.56(5)
O5	2*n*	0.4621(4)	0.3359(2)	1/2	0.56(5)
O6	2*m*	0.6641(2)	0.4621(4)	0	0.56(5)
O7	2*i*	0	0	0.252(2)	0.56(5)

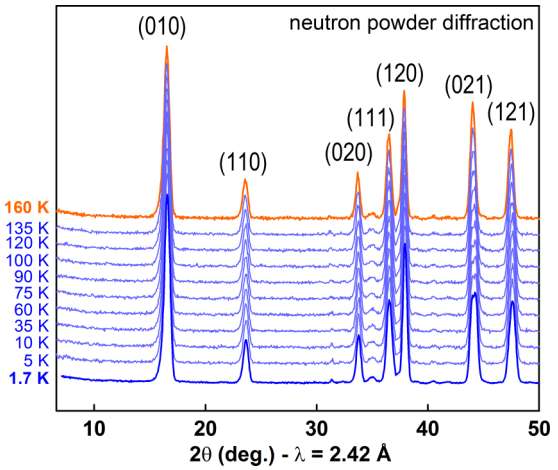

FIG. 9. Evolution of the neutron powder diffraction patterns ($\lambda = 2.42$ Å) of $Li_2Cu_2O(SO_4)_2$ while cooling the sample from 160 K (above the transition) down to 1.7 K. (*hkl*) indexes refer to the tetragonal cell. Note the absence of any peak arising at low angle, nor diffuse background of magnetic origin.

Peierls or spin-driven Jahn-Teller transitions. A spin Peierls driven distortion is however unlikely as this distortion is concomitant with the opening of a gap in the spectrum of magnetic excitations. Indeed, all phases present in the phase diagram of antiferromagnetic spin-1/2 Heisenberg Hamiltonian for an undistorted linked tetrahedra geometry, as exhibited by $Li_2Cu_2O(SO_4)_2$ in its high-temperature structure, are already gapped [22]. Yet, the fact that this transition occurs at the same temperature (125 K) as the broad maximum observed in the magnetic susceptibility also seems to indicate that the structural modifications have an impact on the magnetism of this compound. This is currently being explored by density functional calculations and will be reported in a forthcoming paper.

ACKNOWLEDGMENTS

We thank Yannick Klein for the specific heat measurement and Thomas Hansen for his help during neutron diffraction experiments. We also acknowledge Jean-Marie Tarascon for many fruitful discussions and Antonella Iadecolla for advices. This work was supported by French state funds managed by the ANR within the Investissements d'Avenir programme under reference ANR-11-IDEX-0004-02, and more specifically within the framework of the Cluster of Excellence MATISSE led by Sorbonne Universités.

APPENDIX

Let $\mathbf{r}(\mu)$ be the positions of the atoms $\mu(\mu = 1,\ldots,s)$ within an asymmetric unit of the parent structure with space group **H**. The asymmetric unit of the observed distorted structure with lower symmetry space group **L**, subgroup of **H**, will in general have a larger number of atoms due to the splitting of the Wyckoff orbits in **H**. Thus the atom positions of the structure, described in the subgroup **L**, are given in terms of the atom positions of the parent group **H** described in the basis (unit cell) of the subgroup **L** as

$$\mathbf{r}(\mu,i) = \mathbf{r}_0(\mu,i) + \mathbf{u}(\mu,i), \quad \mu = 1,2,\ldots,s,$$
$$i = 1,2,\ldots,n_\mu; \quad \mathbf{u}(\mu,i) = \sum_{\tau,m} A_{\tau,m}\, \boldsymbol{\varepsilon}(\tau,m|\mu,i).$$

The displacement vectors $\mathbf{u}(\mu,i)$ are written as linear combinations of the polarization modes (basis vectors of the irreducible representations involved in the phase transition). The indices τ and m label all possible distinct allowed symmetry-adapted distortion modes. The index τ stands for the different irreducible representations, while m ($m = 1,\ldots,n_\tau$) enumerates the possible different independent modes within a given representation. The amplitudes $A_{\tau,m}$ are the variable parameters in the refined crystal structure with FULLPROF. In order to enhance the role of the different representations we redefine the displacement vectors as

$$\mathbf{u}(\mu,i) = \sum_{\tau,m} A_{\tau,m}\, \boldsymbol{\varepsilon}(\tau,m|\mu,i) = \sum_{\tau} A_\tau\, \mathbf{e}(\tau|\mu,i),$$

in which the global amplitude of the irreducible representation τ and the new polarization vectors are defined as

$$A_\tau = \left(\sum_m A_{\tau,m}^2\right)^{1/2}$$
$$\mathbf{e}(\tau|\mu,i) = \sum_m a_{\tau,m}\, \boldsymbol{\varepsilon}(\tau,m|\mu,i); \quad a_{\tau,m} = \frac{A_{\tau,m}}{\left(\sum_m A_{\tau,m}^2\right)^{1/2}}$$

Decomposing the structure in terms of the global amplitudes A_τ, we can determine the primary representation responsible for the main distortion of the structure.

[1] C. Lacroix, P. Mendels, and F. Mila, *Introduction to Frustrated Magnetism: Materials, Experiments, Theory* (Springer Science & Business Media, 2011).
[2] J. S. Miller, *Extended Linear Chain Compounds*, Vol. 3 (Springer US, New York, 1983).
[3] A. Seidel, C. A. Marianetti, F. C. Chou, G. Ceder, and P. A. Lee, Phys. Rev. B **67**, 020405(R) (2003).
[4] M. Nishi, O. Fujita, and J. Akimitsu, Phys. Rev. B **50**, 6508 (1994).
[5] M. Hase, I. Terasaki, and K. Uchinokura, Phys. Rev. Lett. **70**, 3651 (1993).
[6] Y. Yamashita and K. Ueda, Phys. Rev. Lett. **85**, 4960 (2000).
[7] M. Sun, G. Rousse, A. M. Abakumov, M. Saubanère, M.-L. Doublet, J. Rodríguez-Carvajal, G. Van Tendeloo, and J.-M. Tarascon, Chem. Mater. **27**, 3077 (2015).
[8] H. M. Rietveld, J. Appl. Crystallogr. **2**, 65 (1969).
[9] J. Rodríguez-Carvajal, FULLPROF Suite www.ill.eu/sites/fullprof/.
[10] J. Rodríguez-Carvajal, Phys. B Condens. Matter **192**, 55 (1993).
[11] D. Orobengoa, C. Capillas, M. I. Aroyo, and J. M. Perez-Mato, J. Appl. Crystallogr. **42**, 820 (2009).
[12] P. Stephens, J. Appl. Crystallogr. **32**, 281 (1999).

[13] See the manual of FULLPROF for the scaling of these parameters to obtain the broadening in 2θ and the way of calculating the strain.

[14] See Supplemental Material at http://link.aps.org/supplemental/10.1103/PhysRevB.95.144103 for obtaining the microstructural information file, the pcr-file, the list of amplitudes, and specific heat and DSC measurements; crystallographic information files (CIF) at 300 K and 2 K are also available.

[15] J. Rodriguez-Carvajal, M. T. Fernandez-Diaz, and J. L. Martinez, J. Phys.: Condens. Matter **3**, 3215 (1991).

[16] J. M. Perez-Mato, D. Orobengoa, and M. I. Aroyo, Acta Cryst. A **66**, 558 (2010).

[17] M. Kofu, J.-H. Kim, S. Ji, S.-H. Lee, H. Ueda, Y. Qiu, H.-J. Kang, M. A. Green, and Y. Ueda, Phys. Rev. Lett. **102**, 037206 (2009).

[18] G. Radtke, A. Saúl, H. A. Dabkowska, G. M. Luke, and G. A. Botton, Phys. Rev. Lett. **105**, 036401 (2010).

[19] A. Carpy and J. Galy, Acta Crystallogr. B **31**, 1481 (1975).

[20] M. V. Mostovoy and D. I. Khomskii, Solid State Commun. **113**, 159 (1999).

[21] T. Ohama, H. Yasuoka, M. Isobe, and Y. Ueda, Phys. Rev. B **59**, 3299 (1999).

[22] M. P. Gelfand, Phys. Rev. B **43**, 8644 (1991).